

Neutron scattering from the Heisenberg ferromagnets EuO and EuS. II. Static critical properties*

J. Als-Nielsen[†] and O. W. Dietrich[†]

Research Establishment Risø, DK 4000 Roskilde, Denmark

L. Passell

Brookhaven National Laboratory, Upton, New York 11973

(Received 13 May 1976)

Neutron scattering has been used to study the magnetic ordering process in the isotropic exchange coupled ferromagnets EuO and EuS. Quantities investigated include the critical coefficients B and F^+ and the critical exponents β , ν , and γ describing respectively the temperature dependence of the reduced magnetization below T_C and the temperature dependence of the inverse spin correlation range and reduced static susceptibility above T_C . All of the above-mentioned parameters are found to be in satisfactory agreement with theoretical predictions; a predicted scaling relation between β , ν , and γ is also confirmed. An approximate procedure for unfolding from the scattering below T_C that part associated with the longitudinal static susceptibility was developed and applied to EuO to obtain an indication of the distance over which longitudinal spin fluctuations are correlated in the ordered state. The results are consistent with the view that the range of spin correlations below T_C is about half as large as at an equivalent temperature about T_C . In all but one case, agreement between the neutron scattering results and those obtained by other experimental methods is within the limits of the errors. The exception is the critical exponent γ for which the neutron value is significantly larger than that derived from bulk measurements.

I. INTRODUCTION

In the first paper of this series we reviewed our low-temperature inelastic-neutron-scattering measurements of spin-wave dispersion in EuO and EuS and discussed their interpretation in terms of magnetic exchange constants. We turn now in this second paper to consideration of our elastic and quasielastic scattering experiments near the Curie temperature T_C , and to the question of what can be learned from these measurements concerning magnetic ordering in EuO and EuS.

As is well known, the magnetic ordering transition is one of a limited class of phase transitions which come under the collective heading of second-order processes. In attempting to describe such processes theoretically, the tendency has been to focus on certain idealized systems which are simple enough to be amenable to detailed analysis and yet at the same time realistic enough to represent actual systems found in nature. Among such systems, the best known is probably the isotropic exchange-coupled Heisenberg magnet.

Relatively few materials can be described as good representations of Heisenberg magnets. Naturally, those which do fit within this select category are of particular interest from the experimental point of view. Thus RbMnF₃, an excellent example of an isotropic Heisenberg antiferromagnet, has been much studied,¹ as have EuO and EuS, the only known examples of Heisenberg ferromagnets. But, for the reasons outlined in the

first paper of this series, although the macroscopic magnetic properties of both EuO and EuS are thoroughly documented, nothing comparable is known about their microscopic behavior.

In this paper we will discuss the application of neutron scattering methods to EuO and EuS to probe, on a microscopic scale, the temperature dependence of long-range magnetic order below T_C and short-range order above T_C . Some of the experimental results to be discussed have already been briefly described in the literature²; here we would like to explain how these measurements were made, and in particular how the data were corrected and analyzed. We will also discuss some previously unreported measurements made on EuO below T_C which represent a first attempt to investigate longitudinal spin fluctuations in an ordered ferromagnetic system.

II. NEUTRON SCATTERING CROSS SECTION

Marshall and Lovesey³ have presented a detailed exposition of the theory of neutron scattering from a Heisenberg magnet with a Bravais lattice. For our purposes it will be sufficient to summarize briefly those aspects of the theory which are relevant to our measurements. The partial differential cross section is customarily written in the form

$$\frac{d^2\sigma}{d\Omega dE'} = \left(\frac{\gamma e^2}{m_e c^2}\right)^2 \frac{k_f}{k_i} \left|\frac{1}{2}gF(\vec{\kappa})\right|^2 \sum_{\alpha} (1 - \vec{k}_{\alpha}^2) S^{\alpha}(\vec{\kappa}, \omega), \quad (1)$$

where the quantity

$$S^\alpha(\vec{k}, \omega) = \frac{1}{2\pi\hbar} \int_{-\infty}^{\infty} dt e^{-i\omega t} \langle \hat{s}_{\vec{k}}^\alpha(0) \hat{s}_{\vec{k}}^\alpha(t) \rangle,$$

known as the dynamic structure factor, represents the Fourier transform of the spin pair correlation function and $\vec{k}_i - \vec{k}_f \equiv \vec{\kappa} = \vec{q} + \vec{\tau}$, where $\vec{\tau}$ is a reciprocal-lattice vector. The notation follows that of Ref. 3. Using linear response theory, $S^\alpha(\vec{\kappa}, \omega)$ can be described in terms of a normalized spectral weight function $F^\alpha(\vec{q}, \omega)$ and a wave-vector-dependent susceptibility $\chi_{\vec{q}}^\alpha$; the relationship takes the form

$$S^\alpha(\vec{\kappa}, \omega) = S_{\text{Bragg}}^\alpha(q=0, \omega=0) + \frac{NS(S+1)}{3\hbar} \frac{\chi_{\vec{q}}^\alpha(T)}{\chi_0} \frac{\hbar\omega\beta}{1 - e^{-\hbar\omega\beta}} F^\alpha(q, \omega). \quad (2)$$

The first term in Eq. (2), representing the magnetic contribution to the coherent Bragg scattering, is proportional to the square of the magnetization M , and is a δ function in both q and ω . The second term describes the inelastic magnetic scattering associated with fluctuations in the local magnetization. As the temperature increases, this term contributes more to the scattering and ultimately, near T_C , it evolves into the intense critical magnetic scattering which is the major subject of this paper.

Let us consider first the elastic magnetic Bragg scattering, which we remarked was proportional to M^2 , and which can be used to determine the temperature variation of the magnetization, i.e., the temperature variation of the long-range magnetic order. Below T_C there are both magnetic and nonmagnetic contributions to the Bragg scattering and both must be taken into account. The nonmagnetic part is associated with coherent nuclear scattering from the rock-salt lattice structure, and it remains essentially constant in intensity over the temperature range of our measurements. This "nuclear background" can be independently determined above T_C and therefore presents no real difficulties. There is, however, also a small contribution to the background from quasielastic critical scattering [the second term in Eq. (2)] which must be taken into account. This will be discussed in detail in Sec. IV E when we consider analysis of the data.

As far as the second term in Eq. (2)—the non-Bragg term—is concerned we note, as was earlier remarked, that this is entirely inelastic magnetic scattering and, in double axis measurements such as those to be described here, the observed intensity will be approximately proportional to the integral of Eq. (1) over all E' , i.e., over the energy

spectrum of the scattered neutrons. The reasons why this is approximately but not exactly true will be discussed in detail in Sec. IV B, but for the moment we will simply assert that the scattered intensity is essentially determined by the quantity $T \sum_{\alpha} (1 - \bar{\kappa}_{\alpha}^2) \chi_{\vec{q}}^{\alpha}$.

Below T_C , the term $\sum_{\alpha} (1 - \bar{\kappa}_{\alpha}^2) \chi_{\vec{q}}^{\alpha}$, takes the form $\frac{2}{3}(\chi_{\vec{q}}^l + 2\chi_{\vec{q}}^t)$, the superscripts l and t identifying, respectively, the longitudinal and transverse components of the susceptibility (defined with respect to the direction of the spontaneous magnetization). According to molecular-field theory,³

$$\chi_{\vec{q}}^l \propto q^{-2} \quad (3)$$

in the small- q limit; the same q dependence also is obtained from more sophisticated theories.⁴ For $\chi_{\vec{q}}^t$, molecular-field theory yields for an isotropic Heisenberg ferromagnet near T_C the expression

$$\chi_{\vec{q}}^t \propto [(a_{\text{nn}}q)^2 + (a_{\text{nn}}\kappa_1)^2]^{-1}, \quad (4)$$

where κ_1 represents the inverse spin correlation range. This expression is also expected to hold in the small- q limit. We have formally introduced the nearest-neighbor (nn) distance a_{nn} into Eq. (4) to emphasize that the correlation range is expected to scale with this quantity in otherwise identical systems.

Kawasaki⁴ has used a diagrammatical technique in the molecular-field approximation to study the form of $\chi_{\vec{q}}^l$ more carefully. His conclusion is that below T_C the longitudinal susceptibility $\chi_{\vec{q}}^l$ consists of two terms; the first proportional to

$$1/a_{\text{nn}}^2(q^2 + \kappa_1^2),$$

and the second to

$$\frac{T_C - T}{T} \left[\frac{1}{a_{\text{nn}}^2(q^2 + \kappa_1^2)} \right]^2 \frac{1}{qa_{\text{nn}}}.$$

At low temperatures the second term is dominant. However, at higher temperatures Kawasaki finds that the first term becomes of increasing importance and ultimately, near T_C , it determines the form of $\chi_{\vec{q}}^l$ except at extremely small values of q . Hence, we can conclude that not far below T_C , in the q range accessible to experiment, $\chi_{\vec{q}}^l$ should retain the Ornstein-Zernike form of Eq. (4).

Above T_C , separation of $\chi_{\vec{q}}$ into longitudinal and transverse components is meaningless. Ritchie and Fisher⁵ suggest, on the basis of series-expansion calculations, that it be expressed as

$$\frac{\chi_{\vec{q}}(T)}{\chi_0} = \left(\frac{\chi_{q=0}(T)}{\chi_0} \right) \left(1 + \frac{\phi q^2}{\kappa_1^2} \right)^{1/2} \left/ \left(1 + \frac{\psi q^2}{\kappa_1^2} \right) \right., \quad (5)$$

where

$$\phi(T) = \phi_c (T_C/T)^3$$

and

$$\psi(T) = 1 + \frac{1}{2}\eta\phi^2(T).$$

The exponent η and the shape parameter ϕ are predicted in Ref. 5 to be numbers on the order of 0.1 or smaller.

Before concluding this brief review, some comment is necessary concerning $F(q, \omega)$, the spectral weight function which also appears in Eq. (2). Clearly in studies of static behavior, χ_q is the object of major interest and $F(q, \omega)$ is only of importance insofar as it affects corrections to the measurements. It is therefore sufficient for our purposes at this time simply to note that at low temperatures $F(q, \omega)$ is expected to be a two-peaked function representing processes in which neutrons gain and lose energy by interactions with spin-wave modes. As T approaches T_C , the energies of the spin waves renormalize and they become increasingly short lived. In addition, longitudinal fluctuations are expected to begin contributing to the scattering. The two spin-wave peaks in $F(q, \omega)$ therefore decrease in energy, broaden, and finally, at T_C , or slightly above, they are expected to merge with the central longitudinal peak into a single peak centered at zero energy transfer. This single peak then continues to broaden as the temperature further increases.

More quantitative descriptions of $F(q, \omega)$ will be found in the third paper of this series, which is concerned with our investigations of spin dynamics in EuO. It is suggested that readers interested in dynamic processes refer to this paper for further details.

III. EXPERIMENTAL METHOD

A. Neutron scattering measurements

Experience shows that to determine static magnetic critical properties accurately, good q resolution and good statistics, i.e., high counting rates are required. For this reason all of the measurements to be discussed were made with a triple-axis spectrometer operated in the two-axis mode. We employed a relatively high incident neutron energy, 13.5 meV ($\lambda = 2.46 \text{ \AA}$), to minimize the importance of corrections for inelasticity. Pyrolytic graphite was used for the monochromating crystal and quartz and pyrolytic graphite filters were incorporated into the beam to remove contamination from higher orders. Horizontal collimation in front of the monochromator, was 0.6° ; between monochromator and sample, 0.42° ; and between sample and detector, 0.29° . Vertical collimations before and after the sample were 0.76° and 0.66° , respectively.

B. Sample arrangement and thermometry

The samples were in the form of slabs of polycrystalline powder. Details of their preparation, weight, and dimensions are given in paper I, Sec. III C.

Temperatures below 30 K were measured with calibrated Ge cryoresistors; at higher temperature calibrated Pt resistance thermometers were employed. As noted in paper I Sec. III C, the ordering temperatures of both the EuO and EuS samples were determined from the scattering at $q = 0.05 \text{ \AA}^{-1}$. The observed values of T_C were $69.15 \pm 0.05 \text{ K}$ for EuO and $16.57 \pm 0.02 \text{ K}$ for EuS.

IV. ANALYSIS OF THE DATA

A. Sources of background and background corrections

As explained in paper I, since the samples were polycrystalline powders, all measurements of the inelastic magnetic scattering [the second term in Eq. (2)] had to be made at small angles around the origin in reciprocal space. Near the forward direction, a recorded count can originate from any of the following processes: (a) inelastic magnetic (critical) scattering from the sample; (b) inelastic nuclear (phonon) or elastic coherent (multiple Bragg) scattering from the sample; (c) elastic nuclear spin incoherent scattering from the sample; (d) scattering from the sample container, cryostat radiation shields, etc., room background, and detector noise.

Process (a) is, of course, the scattering in which we are interested while processes (b)–(d) represent sources of background in our measurements. Of these latter, as will be explained, (c) and (d) could be determined reasonably well while (b) presented difficulties and, for lack of a better means, had to be estimated by inference using a procedure which we will describe.

We can perhaps best make clear the methods used to evaluate these background contributions by discussing our measurements on EuO in detail. Consider first background source (d). This was determined by replacing the sample with a 0.05-mm-thick cadmium sheet selected to give approximately the same neutron transmission. The sample container, cryostat radiation shields, etc., were unchanged. Although Cd is to some extent a scatterer as well as an absorber, the scattering is small enough to be neglected and the observed scattered intensity is therefore almost entirely that from (d) above.

Source (c), the elastic spin incoherent contribution, was determined by using triple-axis spectroscopy. At low temperatures, the spin-wave an-

nihilation and creation peaks are well separated and the incoherent elastic peak is fully resolved and easily identified. At high temperatures the incoherent scattering appears as a well-defined narrow elastic peak on top of a much wider paramagnetic peak. By using the ratio of the incoherent elastic intensity to the total energy-integrated intensity (observed at both high and low temperatures and at various values of q) we were able to obtain reliable estimates of the contribution of incoherent elastic scattering to the intensity observed in our two-axis studies.

The sum of sources (c) and (d) appears in Fig. 1 as the dashed curve labeled "lower limit." On the scale of the figure the incoherent elastic background is 18 counts. The upper dashed curve is the scattered intensity observed from the EuO sample at room temperature ($4T_C$) which includes not only (b)–(d), but also (a), the inelastic paramagnetic scattering as well. Although at room temperature this scattering is much reduced over what it is near T_C and is also essentially independent of q in the range of our measurements ($0.15 > q > 0.05 \text{ \AA}^{-1}$), it is still not completely negligible. Therefore at $4T_C$ the measurement defines in effect an "upper limit" to the background.

Since we could find no direct way of evaluating (b), the phonon and multiple Bragg components of the background, we were forced to resort to an iterative trial-and-error procedure to determine this quantity. The procedure involved analyzing the data with various choices of background between the established upper and lower limits and evaluating the results on the basis of the following criteria:

(i) κ_1 must vanish at $T = T_C$.

(ii) The magnetic contribution to the scattered intensity at room temperature must be essentially independent of q for $q < 0.15 \text{ \AA}^{-1}$.

(iii) $\chi_{q=0}(T)/\chi_0$ and κ_1 must vary smoothly with temperature, i.e., the results at high temperatures, where the background is relatively much more important, must extrapolate in a physically reasonable way to the results near T_C , which are much less dependent on background. Most of the possible choices failed to satisfy one or more of the above criteria. However, the background shown as the solid curve in Fig. 1 met all requirements. In fact, as we will show in Sec. IV C, with this background, $\chi_{q=0}(T)/\chi_0$ actually extrapolates to the expected room-temperature value.

According to our interpretation, the difference between the curve labeled "final background" in Fig. 1 and that labeled "lower limit" is the contribution from (b) as defined above. We believe it comes primarily from multiple Bragg scattering for the following reason. In a nonabsorbing ma-

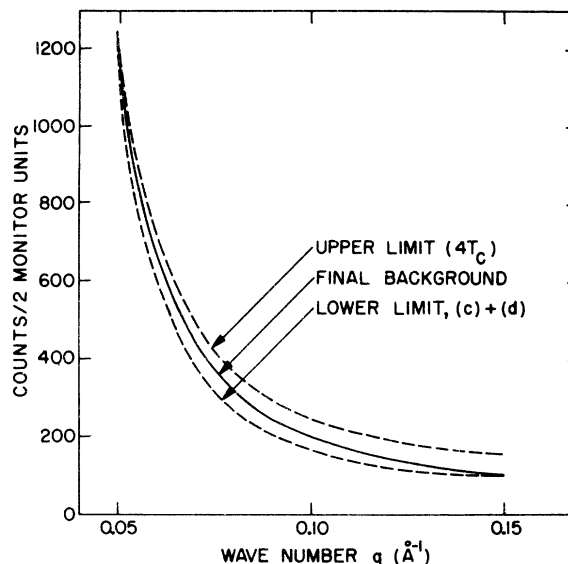


FIG. 1. q dependence of EuO background. The upper dashed curve is the observed scattering from the sample at room temperature; the lower represents the sum of incoherent scattering from the sample and scattering from the sample container, cryostat radiation shields, etc. Together, they define upper and lower limits to the background. The solid line in between is the interpolated background used for analysis of the data.

terial, the intensity of multiple Bragg scattering will vary as $(\sin 2\theta_s)^{-1}$, where $2\theta_s$ is the scattering angle. Strong absorption tends to attenuate the large-angle scattering, hence, in EuO the multiple Bragg contribution can be expected to be more strongly peaked in the forward direction. Careful inspection of Fig. 1 will show that this is consistent with what we observed.

Before leaving the subject of background, one further point ought to be made clear. The procedures we have used to determine the background in EuO and EuS are valid only when (i) temperatures both substantially above and below T_C are experimentally accessible and (ii) the material does not undergo a crystallographic phase transition within this temperature range. This method could not, for example, be applied to iron which has a high value of T_C and which furthermore undergoes a crystallographic phase transition not too far above this temperature.

B. Corrections for inelasticity and experimental resolution

The double-axis mode of operation measures, at each spectrometer setting, the intensity of neutrons scattered through a specific angle, $2\theta_s$. As was mentioned earlier, when inelastic processes produce a spread in the energies of the scattered

neutrons there is a corresponding spread in the q vectors of the neutrons detected. This is indicated schematically in Fig. 2. The range of energy transfers which must be considered is determined by the energy width of the spectral weight function $F(q, \omega)$; the appropriate q vectors being those with endpoints along \vec{k}_f , such as for example $\vec{q}_1, \dots, \vec{q}_3$ in the figure. Let us denote by ΔE_f the characteristic width of the cross section along \vec{k}_f . The equivalent range of scalar momentum of the scattered neutrons Δk_f is

$$\Delta k_f = \frac{\partial k_f}{\partial E_f} \Delta E_f = \frac{1}{\hbar} \left(\frac{m}{2E_f} \right)^{1/2} \Delta E_f.$$

As long as $E_f \approx \hbar^2 k_f^2 / 2m$ is large enough, Δk_f will be small no matter how large the inelasticity, and the scattering will be confined to a narrow range of q values. Thus, in the limit of large neutron

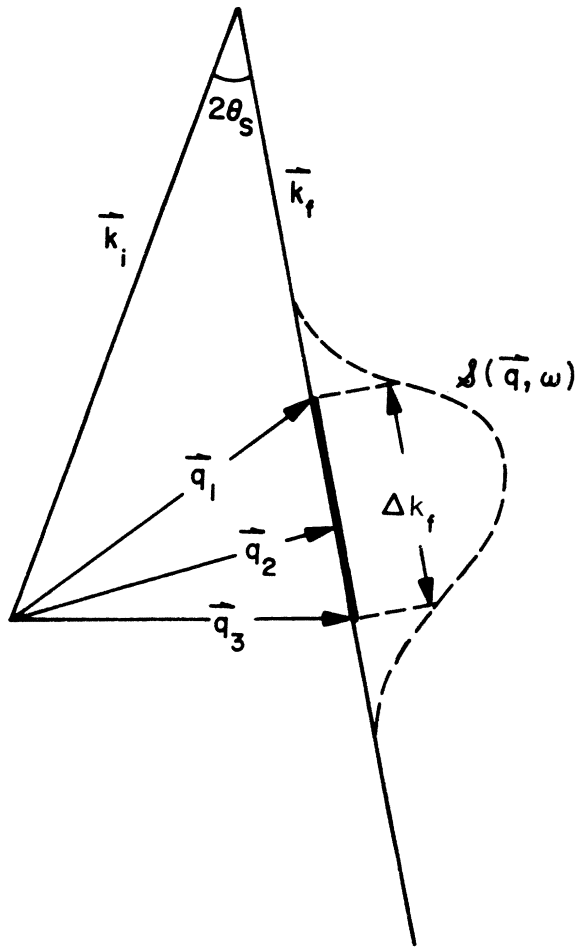


FIG. 2. Scattering diagram for the analysis of double-axis measurements of small-angle scattering. The dashed line indicates the spectral distribution of the scattered neutrons.

energies, the intensity observed with a double-axis spectrometer becomes in effect a measure of the cross section integrated over energy at a fixed q value, i.e., it is proportional to the static susceptibility for magnetic scattering at that value of q , as was noted earlier. Although this limit cannot be completely achieved in practice, the corrections are not large and two-axis measurements are therefore commonly employed for studies of the static susceptibility.

When the form of $F(q, \omega)$ is known, correcting for inelasticity is a straightforward procedure.⁶ The cross section, including the known $F(q, \omega)$ and a parameterized form of $\chi_{\vec{q}}$, is integrated numerically along the direction of \vec{k}_f . Since $F(q, \omega)$ is a normalized function, it is convenient to calculate an "inelasticity correction factor" defined as

$$f(\vec{q}_0) \equiv \frac{\int_{\text{along } k_f} \chi_{\vec{q}} F(q, \omega) d\omega}{\chi_{\vec{q}_0}}.$$

Then, after other corrections have been made, the intensity $I(\vec{q}_0)$ at a spectrometer setting corresponding to elastic momentum transfer \vec{q}_0 will be related to $\chi_{\vec{q}_0}$ by the expression

$$I(\vec{q}_0) = f(\vec{q}_0) \chi_{\vec{q}_0}.$$

Normally, the parameters in the expression for $\chi_{\vec{q}_0}$ are determined by least-squares fitting. Consequently, the inelasticity correction factor has to be calculated for each set of trial parameters used in the fitting process.

In the analysis of our data we assumed $F(q, \omega)$ to be of Lorentzian form in ω , i.e., either a two-peaked or single-peaked function, as was discussed in Sec. II. The width of the Lorentzian $\Gamma(q)$ was obtained from inelastic measurements (to be discussed in paper III). Here we only need mention that the observed q and temperature dependence of $\Gamma(q)$ above T_c followed the predictions of Résibois and Piette.⁷ Therefore, their curve for $\Gamma(q)$ was fitted to our inelastic data and was used to calculate the inelastic correction factor.

The finite instrumental resolution of the spectrometer means that every measurement represents an average of the cross section over a certain "resolution volume" in \vec{q} space. Thus a measurement made at a nominal elastic momentum transfer \vec{q}_0 is in fact a weighted average of $\chi_{\vec{q}}$ around the value \vec{q}_0 : the spread in wave vectors around \vec{q}_0 owing to instrumental resolution being determined by the horizontal and vertical divergence of the spectrometer collimation and the crystal mosaic distributions. In analyzing our data we combined in one calculation the resolution and inelasticity corrections which together did not exceed 10% for any of our measurements.

C. Short-range order above T_C

The results of a preliminary analysis of our data have already been published.² In making this analysis, we assumed a simple Ornstein-Zernike form for $\chi_{q=0}(T)/\chi_0$, i.e., the form obtained from Eq. (5) when η is set equal to 0. Here we present a more-refined analysis based on fitting our data to Eq. (5), the Ritchie and Fisher expression. For ϕ_C we used 0.11, the value given in Ref. 5 for an fcc lattice of spins with $S = \frac{7}{2}$. With this quantity fixed, Eq. (5) then contains three unknowns, namely, $\chi_{q=0}(T)/\chi_0$, κ_1 , and η .

We consider first the determination of η . Because of the angular dependence of the background and the difficulties involved in approaching the limit $q = 0$ in forward-scattering measurements, our results are in general not very sensitive to the value of η . The most favorable situation occurs when $T - T_C$. In this case $\kappa_1 \rightarrow 0$ and it is easy to see from Eq. (5) that $\chi_{q=0}(T_C)/\chi_0 \propto q^{2-\eta}$. Figure 3 shows the product of $q^{2-\eta}$ and the intensity at T_C , i.e., $q^{2-\eta}I(T_C, q)$, plotted against q for two representative values of η . As is evident, the product is not constant when the analysis is made with $\eta = 0$, in other words, when the Ornstein-Zernike form is used. It does, however, remain effectively constant with $\eta = 0.068$. Ritchie and Fisher⁵ predicted for η the value 0.043 ± 0.014 . Considering the possibilities for systematic error in both the measurements and data analysis, the agreement is satisfactory.

The remaining quantities to be determined are $\chi_{q=0}(T)/\chi_0$ and κ_1 . Figure 4 shows least-squares fits to the data at $\Delta T/T_C = 0.020$ and 0.102 with η held fixed at the Ritchie and Fisher value of 0.043 , i.e., with only $\chi_{q=0}(T)/\chi_0$ and κ_1 considered to be parameters of the fit. In the figure, the open circles represent the observed intensities with background subtracted. Also included for purposes of comparison are the background (the dash-dotted curve) and χ_q/χ_0 at $\Delta T/T_C = 0.020$ (the dashed curve). The solid lines represent χ_q/χ_0 folded with the inelasticity and instrumental resolution. It is clear from Fig. 4 that background corrections are far more important than corrections for inelasticity and instrumental effects.

Tables I and II give the results for $\chi_{q=0}(T)/\chi_0$ and κ_1 for EuO and EuS, respectively. We have listed not only the best-fitting values obtained with $\eta = 0.043$ but also those obtained with $\eta = 0$ to show how little the results are influenced by variations in this parameter. The second column in Table I shows the extent to which $\chi_{q=0}(T)/\chi_0$ is shifted by decreasing the background by eight counts, the estimated systematic uncertainty in this quantity.

$\chi_{q=0}(T)/\chi_0$, as given in Tables I and II, was

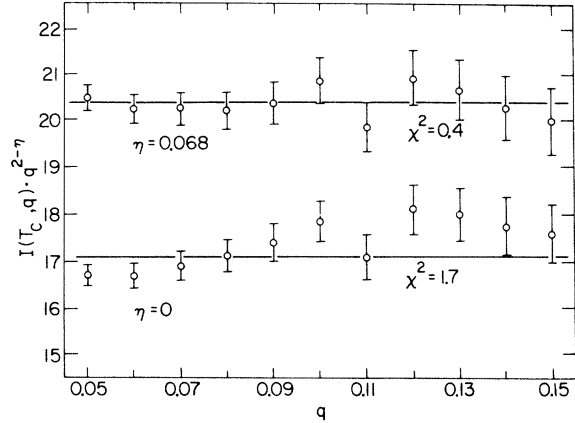


FIG. 3. Intensity of the scattering from EuO at T_C multiplied by $q^{2-\eta}$ and plotted against q for two values of η . The plots are intended to show the sensitivity of the fit to changes in the value of η .

also least-squares fitted to a power law of the form

$$\chi_{q=0}(T)/\chi_0 = C^*[(T - T_C)/T]^{-\gamma}. \quad (6)$$

From this we obtained for the critical exponents the values

$$\gamma = 1.387 \pm 0.036 \text{ for EuO}$$

and

$$\gamma = 1.399 \pm 0.040 \text{ for EuS.}$$

Error limits were assigned on the basis of three assumed major sources of uncertainty: (i) statistical uncertainty from the fitting (± 0.023), (ii) uncertainty in the value of T_C (± 0.025), and (iii) uncertainty in the background (± 0.013). It should be

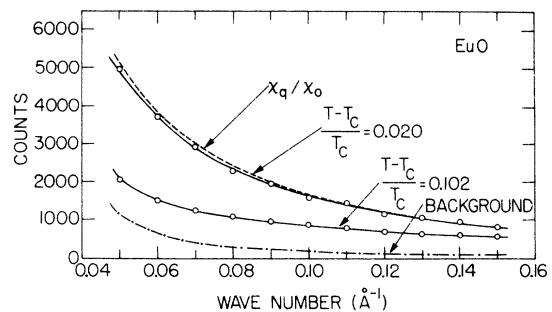


FIG. 4. Best fits of Eq. (5) to the EuO data at $\Delta T/T_C = 0.020$ and 0.102 . The open circles represent the intensities with background subtracted. The dashed curve is χ_q/χ_0 at $\Delta T/T_C = 0.02$; the solid lines are best fits to the data after folding χ_q/χ_0 with the instrumental resolution and inelasticity. The dash-dotted curve is the interpolated background (the solid line in Fig. 1) used in the analysis.

TABLE I. $\chi_{q=0}(T)/\chi_0$ and κ_1 for EuO.

Temperature (K)	$\chi_{q=0}(T)/\chi_0$ $\eta = .043$		$\kappa_1(\text{\AA}^{-1})$		
	Final background	Background -8	$\eta = 0$	$\eta = 0.43$	$\eta = 0$
69.82	22 140 ± 1330	21 700	21 860	0.0280 ± 0.0010	0.0283
70.10	16 470 ± 1310	16 190	16 350	0.0322 ± 0.0015	0.0324
70.55	8 995 ± 489	8 905	8 969	0.0442 ± 0.0016	0.0443
71.25	5 620 ± 360	5 582	5 613	0.0550 ± 0.0025	0.0551
71.76	3 820 ± 159	3 806	3 818	0.0676 ± 0.0023	0.0887
72.63	2 372 ± 64	2 372	2 372	0.0887 ± 0.0023	0.0677
74.01	1 662 ± 62	1 664	1 662	0.104 ± 0.004	0.104
76.20	1 057 ± 30	1 062	1 057	0.131 ± 0.005	0.131
78.81	695 ± 18	702	695	0.165 ± 0.007	0.165
83.00	458 ± 23	465	458	0.211 ± 0.021	0.211
103.80	153 ± 14	160	153	0.46 ± 0.17	0.46

noted that the above error estimates are for EuO. They are, however, expected to apply approximately to EuS as well.

A log-log plot of $\chi_{q=0}(T)/\chi_0$ vs $\Delta T/T$ appears in Fig. 5. Note that for EuO, where the measurements extend over the largest temperature range, the straight-line fit is extremely good even at the highest temperature, i.e., $1.5T_C$. It should be remarked that since the upper limit of the abscissa, $(T - T_C)/T = 1$, corresponds to an infinite temperature, only 0.5 of a decade in $(T - T_C)/T$ has been left unexplored. This was the region, however, in which the background measurements of Fig. 1 were made. It is interesting that the point plotted as the cross in Fig. 5 representing the room-temperature paramagnetic scattering, i.e., the difference between the curves labeled "upper limit" and "final background" in Fig. 1, lies on the extrapolated power law. At first sight it might seem surprising that a single power law applies over so wide a temperature range. In fact, however, the value of the critical coefficient C^* in Eq. (6) is predicted by theory to be close to unity. Since the left-hand side of this expression must, by definition, approach unity in the limit $T \rightarrow \infty$, it is evident that even at high temperatures the extrapolation of Eq. (6) cannot be expected to deviate

TABLE II. $\chi_{q=0}(T)/\chi_0$ and κ_1 for EuS.

Temperature (K)	$\chi_{q=0}(T)/\chi_0$	$\kappa_1(\text{\AA}^{-1})$
16.92	18 360 ± 2000	0.0364 ± 0.0026
17.07	11 190 ± 534	0.0466 ± 0.0015
17.30	6 201 ± 205	0.0631 ± 0.0018
17.74	3 508 ± 149	0.0844 ± 0.0032
18.23	2 195 ± 57	0.1128 ± 0.0032
19.06	1 333 ± 51	0.138 ± 0.007

from the correct value of $\chi_{q=0}(T)/\chi_0$ by more than the difference between C^* and unity. According to Ritchie and Fisher⁵ this difference should be on the order of $\frac{1}{10}C^*$ or less. Thus we find that by using the background of Fig. 1 we have obtained an internally consistent result over the entire temperature range under investigation.

Finally, before leaving this subject, we should

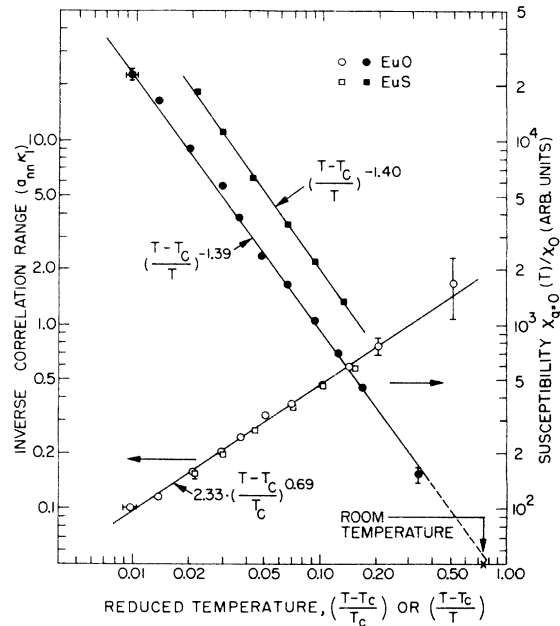


FIG. 5. Reduced temperature dependence of the susceptibility and inverse spin correlation range of EuO and EuS above T_C . Note that the spin correlation ranges of EuO and EuS scale with a_{nn} , the nn distance. The single point plotted as a cross represents the paramagnetic scattering observed at room temperature. The reduced temperature scales for $a_{nn}\kappa_1$ and $\chi_{q=0}(T)/\chi_0$ are $T - T_C/T_C$ and $T - T_C/T$, respectively.

mention that we were not able to obtain a reliable value for C^* experimentally. Its measurement requires an absolute determination of the magnetic cross section; a difficult problem in the presence of absorption as large as that in EuO.

Turning now to the inverse spin correlation range κ_1 , the temperature dependence of this quantity is also expressed in terms of a power law which customarily takes the form

$$a_{nn}\kappa_1 = F^*[(T - T_C)/T_C]^\nu, \quad (7)$$

where a_{nn} is defined to be the nearest-neighbor distance (3.64 Å for EuO and 4.22 Å for EuS). Note, however, that in this case T_C rather than T appears in the denominator so that $a_{nn}\kappa_1$ will extrapolate to the correct limit (infinity) as $T \rightarrow \infty$.

Least-square fits of the measured values of κ_1 to Eq. (7) gave us the following for ν and F^* :
for EuO,

$$\nu = 0.681 \pm 0.017,$$

$$F^* = 2.32 \pm 0.13;$$

and for EuS,

$$\nu = 0.702 \pm 0.022,$$

$$F^* = 2.33 \pm 0.13.$$

The sources of error are the same as those discussed earlier in conjunction with the determination of γ .

The data are plotted in Fig. 5. Note that the inverse spin correlation range scales with the nearest-neighbor distance a_{nn} as expected.

D. Short-range order below T_C

Figure 6 shows the temperature dependence of the two-axis intensity observed below T_C at small values of q . We call attention to the fact that what is plotted in the figure is $I(T)/T$, where $I(T)$ represents the intensity corrected for background, instrumental resolution, and inelasticity. Thus normalized, $I(T)$ is directly proportional to $\chi_q^2(T)$ since the temperature dependence of χ_0 is explicitly taken into account.

We remarked earlier that below T_C it is necessary to consider the scattering as coming partly from the transverse and partly from the longitudinal components of the susceptibility. What is of interest below T_C is the correlation range associated with χ_q^2 , i.e., with the longitudinal part of χ_q^2 , since this is the term which exhibits divergent behavior as $T \rightarrow T_C$. Unfortunately, unless a polarization analysis can be made it is impossible to separate the scattering below T_C into its transverse and longitudinal components experimentally.

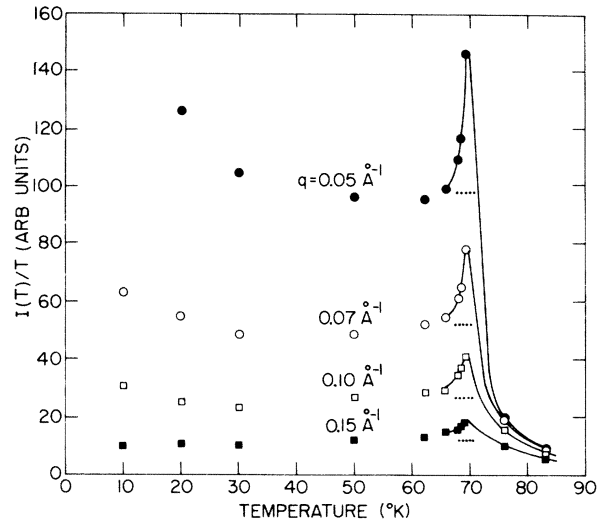


FIG. 6. Intensity of scattering from EuO divided by T and plotted against T for various values of q to show the temperature range over which the scattering is proportional to T . The dotted lines indicate $\frac{2}{3}$ of the intensity at T_C ; the solid lines serve only as a guide to the eye.

Therefore, about the best that can be done is to make use of the fact that since χ_q^2 and χ_q^2 become indistinguishable above T_C , the transverse scattering must, at T_C , be two-thirds of the total observed. Furthermore, as was remarked in Sec. II, there are theoretical reasons for believing that χ_q^2 is not, in the first approximation, a temperature-dependent quantity. Assuming this to be so, it then follows that the scattering below T_C coming from the longitudinal susceptibility can be identified (at least approximately) by subtracting from the quantity $I(T)/T$ plotted in Fig. 6 an amount equal to two-thirds of its value at T_C . According to Eq. (2), this quantity, i.e., $I(T)/T - 2I(T_C)/3T_C$, will then be proportional to χ_q^2 . In Fig. 7 we have plotted $1/\chi_q^2$, as so determined, versus q^2 . It is evident that the data fit the linear relationship expected from Eq. (4) reasonably well. If we use the data at T_C to define the slope, then the data at lower temperatures yield for κ_1 the values appearing in the inset to the figure. Note that for a given $\Delta T/T_C$, the inverse correlation range appears to be about 2.4 times larger below T_C than above. The uncertainty in this number is difficult to estimate since it arises at least as much from the approximations introduced in the analysis as from actual statistical scatter in the data.

If our analysis is consistent, it should follow that the scattering observed at temperatures below about $0.93T_C$ comes from χ_q^2 alone and, therefore, according to Eqs. (2) and (3) should be proportional to T/q^2 . The low-temperature measure-

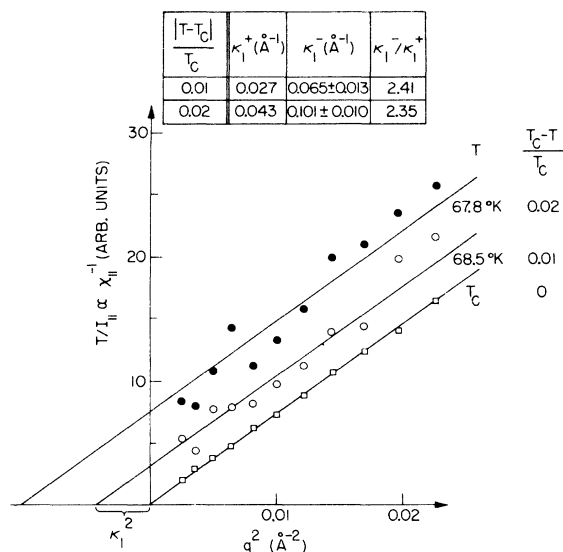


FIG. 7. Plot of $T/I_{||}$ vs q^2 for EuO in the temperature range $T_C \geq T \geq 67.8$ K. $I_{||}$ represents the scattered intensity associated with the longitudinal component of the susceptibility obtained by subtracting from the observed I/T an amount equal to $\frac{2}{3}$ of its value at T_C . The solid lines are best fits of Eq. (4) to the data.

ments, plotted in Fig. 8, indicate that the expected q^{-2} dependence is observed but it is evident from both Figs. 6 and 8 that the intensity of the scattering is not proportional to T as expected. There is clearly extra scattering at low temperatures and small values of q .

We have been unable to identify fully the source of this additional scattering. Triple-axis scans indicate that it is elastic or quasielastic in character. Quite probably it arises from multiple-refraction effects associated with the formation of magnetic domains although this cannot be established with certainty from the available data.

E. Temperature dependence of the magnetization

In Sec. II we noted that the magnetic elastic Bragg scattering occurring below T_C is proportional to the square of the spontaneous magnetization M . It was also remarked that only part of the elastic Bragg scattering is magnetic in origin and that there are other processes contributing to the intensity observed in a two-axis measurement. These must be identified and subtracted as background before the observed intensity can be directly correlated with M^2 . The most important sources of background are (a) nonmagnetic Bragg scattering associated with coherent nuclear reflections from the rock-salt lattice and (b) inelastic magnetic scattering. Let us consider how these back-

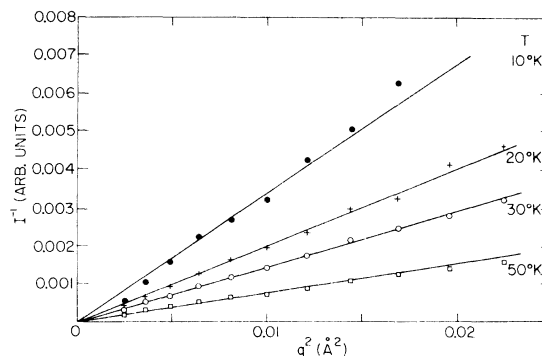


FIG. 8. Plot of the reciprocal of the intensity of scattering from EuO vs q^2 for temperatures ≤ 50 K. The quantity plotted is the observed intensity with background subtracted. The solid lines are straight lines drawn through the points as a guide to the eye.

ground contributions can be isolated and how appropriate corrections can be made to the data.

As far as the first of these background components, i.e., (a), is concerned, we chose the (111) reflection for study because the nonmagnetic nuclear Bragg scattering is relatively smallest for this reflection. Often (and this is the case with both EuO and EuS) the nuclear contribution to the Bragg scattering can be identified simply by raising the sample temperature above T_C so that all of the magnetic elastic scattering disappears. What then remains is simply the scattered intensity associated with (a) plus a small contribution from (b). Assuming that above T_C we can identify and remove the contribution from (b) to obtain (a) alone; then, as we will show, we have effectively determined the nuclear Bragg intensity (a) not only above T_C but also at any temperature below T_C as well. It is easy to understand why this is so.

The intensity of the nuclear Bragg scattering is proportional to the square of the nuclear structure factor, F , which, for the (111) reflection in EuO, is of the form

$$F = 4(b_{\text{Eu}}e^{-W_{\text{Eu}}} - b_0e^{-W_0}).$$

In this expression b_i represents the nuclear scattering amplitude and e^{-W_i} the Debye-Waller factor for each atomic species. All of the temperature dependence of F is contained in W_i , a quantity which can be calculated if the Debye temperature Θ^D is known for each component. From specific-heat measurements in EuO, Teaney⁸ has estimated that $\Theta_{\text{Eu}}^D = 175$ K and $\Theta_0^D = 560$ K. Using these values we find that neither $e^{-W_{\text{Eu}}}$ nor e^{-W_0} departs from unity by more than 1% in the temperature range under study. Therefore we can safely assert that the nuclear Bragg scattering from EuO is effec-

tively constant over the temperature range of interest here. There is no reason to expect that this will not also be the case for EuS as well.

To explain how (a) and (b) were separated above T_C , let us once again concentrate on EuO. Our first step was to measure as accurately as possible the (111) intensity at several temperatures above T_C . To be specific, at $(T - T_C)/T_C = 0.05$ we obtained 268 ± 0.5 counts per unit monitor count and at $(T - T_C)/T_C = 0.10$, 263 ± 0.5 counts per unit monitor count. Since we knew from the argument outlined above that the nuclear Bragg intensity did not vary significantly over this temperature range, we could safely assume that the difference between the two measurements, i.e., 5 ± 0.7 counts per unit monitor count, was due entirely to the temperature dependence of (b), the inelastic magnetic scattering, or in other words, it represented $I_{0.05}^{im} - I_{0.10}^{im}$. As we will explain, our triple-axis studies (described in paper III) allowed us to characterize the inelastic scattering from EuO both above and below T_C well enough so that we could compute the ratio $I_{0.05}^{im}/I_{0.10}^{im}$. From this computed ratio and the observed difference, $I_{0.05}^{im} - I_{0.10}^{im}$, we obtained the values of $I_{0.05}^{im}$ and $I_{0.10}^{im}$ individually. Once I^{im} , the inelastic magnetic contribution, was determined and subtracted from the observed intensity, what remained was assumed to be the nuclear Bragg scattering plus background from air scattering, detector noise, and the like.

Without going into detail, it may be helpful to describe briefly what was involved in computing the ratio $I_{0.05}^{im}/I_{0.10}^{im}$. In two-axis measurements such as the ones we made, the arrangement is as shown schematically in Fig. 9. The spectrometer scattering angle $2\theta_s$ is set so that elastic scattering occurs when $\vec{k} = \vec{k}_i - \vec{k}_f = \vec{\tau}$. But since all neutrons scattered in the direction of \vec{k}_f are detected, there is, in addition to the elastic scattering, an unwanted contribution from inelastic processes. The situation is somewhat similar to that discussed in Sec. IV B, except that in this instance the spectrometer is set, not near the forward direction, but rather at a powder Bragg reflection where the reciprocal-lattice points are distributed over the surface of a sphere of radius τ . In Sec. IV B we were concerned with small-angle scattering about the 000 Bragg point. Here we are dealing with a spherical distribution of reciprocal-lattice points and there are many more possibilities for inelastic processes. As is evident in Fig. 9, for a specific energy transfer, $(\hbar^2/2m)(k_i^2 - k_f^2)$, momentum can be conserved, i.e., $\vec{k}_i - \vec{k}_f = \vec{\tau} + \vec{q}$, for a continuous distribution of wave vectors such as for example q_1 and q_2 . The contribution to the intensity from each q is proportional to the inter-

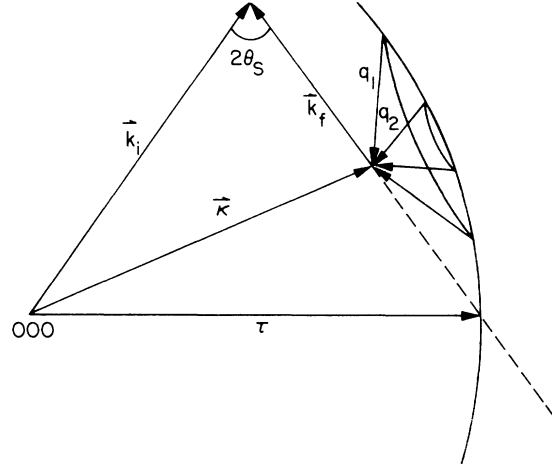


FIG. 9. Scattering diagram showing how inelastic scattering processes in a powder sample contribute to the intensity observed in the double-axis configuration when the spectrometer is set for an elastic reflection at τ .

section of a sphere of radius q , centered at the endpoint of \vec{k}_i , with a sphere of radius τ centered at 000. (In principle, other nearby τ spheres could also contribute to the inelastic scattering, however, in practice these contributions can be neglected because the cross section discriminates strongly against processes involving large momentum or energy transfers.) Thus to evaluate the inelastic contribution to the scattering, a triple integration of the cross section [Eq. (2)] must be made over energy transfers along \vec{k}_f , over wave vectors \vec{q} , and over the circle of intersection mentioned above. The ratio of two such integrations [using in Eq. (2) values of the cross-section parameters appropriate to $(T - T_C)/T_C = 0.05$ and 0.10, respectively], gave us 1.20 as the value of $I_{0.05}^{im}/I_{0.10}^{im}$. Combining this with the measured difference $I_{0.05}^{im} - I_{0.10}^{im} = 5$, we then obtained for $I_{0.05}^{im}$ the value 29 ± 5 counts per unit monitor count and for $I_{nuc1+bgad}$ the value 239 ± 5 counts per unit monitor count. Since we also studied the inelastic scattering below T_C and knew (at least approximately) the form of the cross section, the same numerical approach was used to extrapolate the inelastic contribution to the scattering below T_C . The results are shown in Fig. 10. Note that the total inelastic magnetic intensity varies smoothly through T_C and is not strongly influenced by the divergence associated with longitudinal spin fluctuations.

Although the above analysis was only carried through in detail for EuO it was assumed to apply equally well to EuS. Therefore in analyzing the data for EuS we used the relative variation of I^{im} shown in Fig. 10, but scaled according to mea-

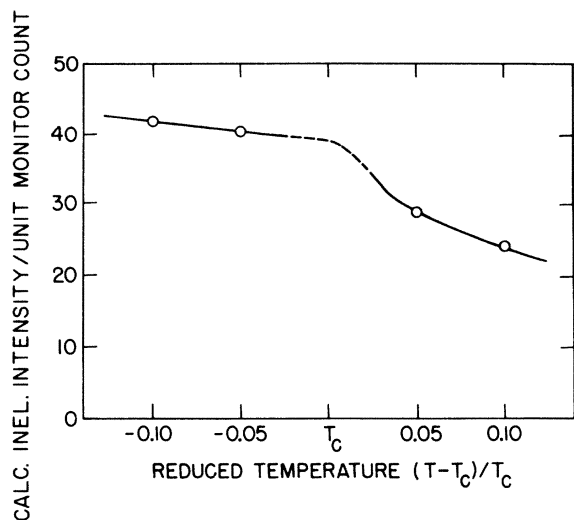


FIG. 10. Calculated inelastic magnetic contribution to the intensity observed with a double-axis spectrometer set for the (111) powder reflection in EuO.

measurements made above T_C in EuS.

There are several more points concerning corrections to the data about which some comment should be made. First, there is the question of extinction. Normally, extinction effects are a source of serious difficulty when Bragg scattering is studied in single crystal samples. In our case, however, thin powder samples were employed and therefore extinction could be ignored. Second, it should be noted that our measurements of the (111) Bragg intensity were not extended to temperatures below 4.5 K. We, therefore, used the results of our studies of spin-wave renormalization (des-

cribed in paper III) to extrapolate the measurements to 0 K to determine the saturation magnetization M_0 .

The resulting reduced magnetizations M/M_0 for EuO and EuS are given in Table III. Listed in the columns labeled I_{total} are the observed (111) intensities together with the appropriate uncertainties due to counting statistics. In the columns labeled $I_{Bragg,magn}$ we have subtracted from I_{total} the nuclear inelastic magnetic and other sources of background and adjusted the uncertainties accordingly. It should be noted that the uncertainties in the columns labeled M/M_0 include (for reasons of convenience in fitting) the uncertainty in the ordering temperature T_C .

To obtain the critical parameters from the observed values of M/M_0 the measurements are fitted to a power law of the form

$$\frac{M}{M_0} = B \left(\frac{T_C - T}{T_C} \right)^\beta. \quad (8)$$

Using the data for $(T_C - T)/T_C \lesssim 0.11$ we found for EuO

$$B = 1.17 \pm 0.02,$$

$$\beta = 0.36 \pm 0.01,$$

and for EuS

$$B = 1.18 \pm 0.03,$$

$$\beta = 0.36 \pm 0.01.$$

Figure 11 shows the result. As would be expected the power law fits well near T_C but fails at lower temperatures.

The reduced magnetization can also be calculated

TABLE III. Reduced magnetization in EuO and EuS.

EuO					EuS				
T (K)	$\frac{T_C - T}{T_C}$	I_{total}	$I_{Bragg,magn}$	$\frac{M}{M_0}$	T (K)	$\frac{T_C - T}{T_C}$	I_{total}	$I_{Bragg,magn}$	$\frac{M}{M_0}$
4.63	0.933	2657 ± 14	2412 ± 15	0.997 (fix)	4.31	0.740	3006 ± 28	2366 ± 32	0.960 (fix)
35.00	0.494	2106 ± 12	1856 ± 13	0.875 ± 3	6.63	0.600	2765 ± 26	2118 ± 30	0.908 ± 6
49.11	0.290	1556 ± 15	1291 ± 16	0.729 ± 4	8.29	0.500	2541 ± 25	1886 ± 29	0.857 ± 7
57.07	0.175	1209 ± 6	929 ± 8	0.619 ± 2	9.94	0.400	2344 ± 24	1679 ± 28	0.809 ± 7
61.70	0.108	939 ± 10	658 ± 11	0.521 ± 4	11.60	0.300	2124 ± 23	1444 ± 27	0.750 ± 7
63.29	0.0850	824 ± 9	544 ± 10	0.474 ± 4	13.26	0.200	1777 ± 16	1077 ± 22	0.648 ± 7
64.54	0.0670	745 ± 10	465 ± 11	0.438 ± 6	14.75	0.110	1422 ± 18	725 ± 23	0.531 ± 8
65.54	0.0525	672 ± 7	393 ± 9	0.402 ± 5	15.15	0.0858	1311 ± 18	616 ± 23	0.490 ± 9
66.33	0.0410	611 ± 8	332 ± 9	0.370 ± 6	15.45	0.0676	1220 ± 11	526 ± 18	0.453 ± 8
66.86	0.0334	563 ± 7	285 ± 9	0.343 ± 7	15.68	0.0535	1129 ± 11	437 ± 18	0.413 ± 8
67.41	0.0255	498 ± 7	221 ± 9	0.302 ± 8	15.89	0.0410	1043 ± 11	352 ± 18	0.370 ± 9
67.79	0.0200	462 ± 3	185 ± 6	0.276 ± 9	16.04	0.0322	977 ± 8	288 ± 17	0.335 ± 10
68.14	0.0147	428 ± 2	152 ± 6	0.250 ± 13	16.16	0.0247	945 ± 8	257 ± 17	0.316 ± 10
68.48	0.0100	385 ± 6	109 ± 8	0.212 ± 22	16.25	0.0193	910 ± 8	223 ± 17	0.294 ± 11
					16.33	0.0143	849 ± 8	162 ± 17	0.251 ± 13

self-consistently from spin-wave theory using a method employed by Low⁹ which is described in Sec. II A 1 of paper III. For EuO and EuS the self-consistent theory yields, respectively, the solid and dash-dotted lines in Fig. 11. Within its range of convergence ($T < 0.9T_C$) it is evident that this approach provides a remarkably good description of the experimental observations. In addition there is a substantial region of overlap (0.7–0.9 T_C) in which the power-law and spin-wave calculations are in good agreement.

V. COMPARISONS WITH OTHER EXPERIMENTS

Considering first EuO, we are aware of four studies of bulk magnetic properties which give information on the critical parameters. These include Høg and Johansson's measurements¹⁰ made with a vibrating-sample magnetometer; Menyuk, Dwight, and Reed's vibrating-coil-magnetometer experiments¹¹; Groll's studies¹² using the Mössbauer effect; and Huang and Ho's investigations of Faraday rotation.¹³ The results are summarized in Table IV.

Aside from the present measurements, the only investigation of the critical properties of EuS of which we are aware is Heller and Benedek's NMR study of the magnetization below T_C .¹⁴ Their results also appear in Table IV.

In general, the experimental agreement on the values of β and B is within the quoted limits of error. The only possible exception is Heller and Benedek's value of β which might be slightly outside the range of the statistical uncertainties. As far as γ is concerned, however, the neutron scattering results yield values significantly larger than those obtained from bulk magnetization measurements.

It is difficult to account for this disagreement. The fact that the same value of γ has been obtained from three independent studies of bulk magnetic properties makes it hard to believe that these measurements are significantly in error. On the other hand, as was explained in Secs. IV A and IV B, we have been at great pains to look for possible sources of systematic error in our experiments and have found nothing which could explain the difference. Barring the possibility of some as yet undetected systematic error in one or the other type of experiment, we can only suggest that the difficulty might originate from the fact that $\chi_{q=0}(T)/\chi_0$ is obtained from the neutron data by extrapolating to $q=0$ from finite values of q using an assumed form for $\chi_q(T)/\chi_0$, while bulk magnetization measurements are made, in effect, at $q=0$. Although there is no direct evidence linking this procedure to the discrepancy, it is at least

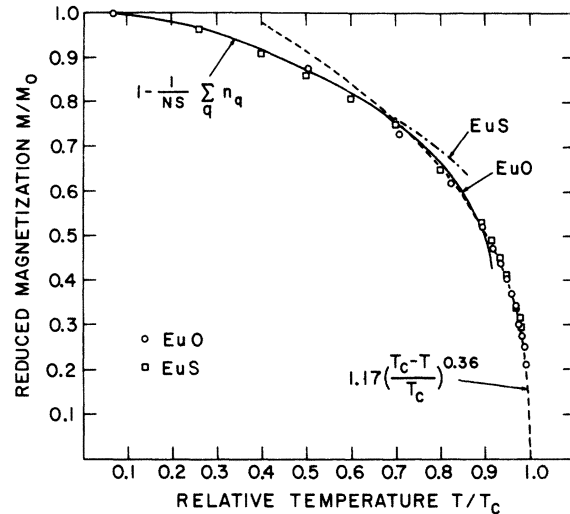


FIG. 11. Temperature dependence of the reduced magnetization of EuO and EuS. The solid and dash-dotted curves were calculated using self-consistent spin-wave theory.

worthwhile to call attention to the fact that the two measurements could be reconciled if Eq. (5) is in some way inappropriate at the smallest values of q . We will have more to say on this point in Sec. VI.

VI. COMPARISONS WITH THEORY

It is generally accepted that for magnetic systems the most accurate results computed from theory are those involving series expansions as, for example, the susceptibility series. In such a series, J/kT is the expansion variable. As is well known, although the convergence of the susceptibility series is poor at temperatures near the ordering temperature, results valid in the critical region can be obtained either by forming successive ratios of expansion coefficients¹⁵ or by using Padé approximants.¹⁶ Series expansions of this type are therefore commonly used to calculate such quantities as $T_C(J)$ [see, for example, paper I, Eq. (7)], C^* and γ [the critical coefficient and exponent in Eq. (6) of this paper], and $\chi_q(T)$, the wave-vector-dependent susceptibility. Alternatively, by expanding in terms of kT/J , series expansions can also be developed for the computation of related quantities below T_C such as the magnetization and the wave-vector-dependent susceptibility.

Listed in the next to last column in Table IV are the currently accepted values for the critical parameters of the isotropic Heisenberg ferromagnet as computed from series expansions. It should be noted that all of the quantities in the table repre-

TABLE IV. Comparison of static critical parameters of EuO and EuS derived from the present neutron scattering measurements with those obtained by other methods and with theoretical predictions for the isotropic Heisenberg ferromagnet.

Expression	Temperature	Quantity	Material	Hyperfine field	Experiments			Theory		
					Faraday rotation	Bulk magnetization	Neutron scattering	Series expansions	Renormalization group, ϵ^2 expansions	
$\frac{M}{M_0} = B \left(\frac{T_C - T}{T_C} \right)^\beta$	$T < T_C$	β	EuO	0.34 ± 0.02^c	0.370 ± 0.006^e	0.368 ± 0.005^a 0.385 ± 0.008^b -0.028	0.36 ± 0.01	0.38^h	0.380^f	
		B	EuS	0.33 ± 0.02^d			0.36 ± 0.01			
			EuO		1.10 ± 0.04^e	1.22^a 1.255 ± 0.030^b -0.100	1.17 ± 0.02	1.12^h		
			EuS	1.145 ± 0.020^d			1.18 ± 0.03			
		γ'	EuO			1.30 ± 0.10^b				
$\frac{\chi_{q=0}(T)}{\chi_0} \propto \left(\frac{T_C - T}{T} \right)^{-\gamma'}$	$T < T_C$	γ'	EuO		1.30 ± 0.02^e	1.29 ± 0.01^a 1.315 ± 0.015^b	1.387 ± 0.036	1.375 ± 0.02^g -0.01	1.365^f	
$\frac{\chi_{q=0}(T)}{\chi_0} \propto \left(\frac{T - T_C}{T} \right)^{-\gamma}$	$T > T_C$	γ	EuO							
$a_{\text{un}^k i} = F^* \left(\frac{T - T_C}{T_C} \right)^\nu$	$T > T_C$	2ν	EuS				1.399 ± 0.040			
			EuO				1.362 ± 0.034	1.405 ± 0.02^g -0.01	1.375^f	
		F^*	EuS				1.404 ± 0.044			
			EuO				2.32 ± 0.13	2.390 ± 0.002^g		
			EuS				2.33 ± 0.15			
		$\beta - \frac{3\nu - \gamma}{2}$	EuO				0.03 ± 0.05		Scaling [†] 0.0	
		$\beta - 1 + \frac{\gamma + \alpha}{2}$	EuS				0.007 ± 0.05			
			EuO				0.03 ± 0.03^j		0.0	
		F^*/F^*	EuO				2.4		2.02	

^aN. Menyuk, K. Dwight, and T. B. Reed, Ref. 11.
^bJ. Högl and T. Johansson, Ref. 10.
^cG. Groll, Ref. 12.
^dP. Heller and G. Benedek, Ref. 14.
^eC. C. Huang and J. T. Ho, Ref. 13.
^fA. D. Bruce and A. Aharony, Ref. 22.
^gD. S. Ritchie and M. E. Fisher, Ref. 5.
^hK. L. Stephenson and P. J. Wood, Ref. 25.
ⁱH. E. Stanley, Ref. 26.
^j $\alpha = -0.04$, A. Kornblit, G. Ahlers, and E. Buehler, Ref. 29.

sent values computed for an isotropic spin- $\frac{7}{2}$ Heisenberg system with only nearest-neighbor interactions.

A different and more general approach to the analysis of critical phenomena has been introduced within the last few years by Wilson¹⁷ who applied renormalization-group theory to the Widom-Kadanoff^{18,19} scaling hypothesis. Although the first results obtained from Wilson's theory were not as accurate as the earlier series-expansion computations, Wilson and Fisher²⁰ have recently shown that comparable accuracy can be achieved from the renormalization-group approach by formally treating the dimensionality d of the lattice as a continuous variable and expanding in terms of the quantity $\epsilon = 4 - d$. The results of such computations appear in the last column of Table IV. Agreement between "renormalization-group" and "series-expansion" calculations is uniformly excellent, as is evident.

Comparisons between experimental results and theoretical predictions are also generally satisfactory both above and below T_C . As is apparent from Table IV, with but one exception the experimentally observed values of the critical parameters agree with the predictions of theory to within the limits of the errors. One notes that the expected scaling relationships between β , γ , and ν are also confirmed. The only point of difficulty is the value of γ ; the neutron scattering results matching the theory while the bulk measurements do not.

We remarked in Sec. V that this puzzling disagreement implies either an unknown source of systematic error in one (or both) experimental approaches and in the theoretical predictions or, alternatively, an incorrect interpretation of one (or both) experiments. It might be argued, as Arrott, Heinrich, and Noakes²¹ and others have done, that the problem results from the influence of dipolar interactions on the long-wavelength magnetic fluctuations, since such interactions are not incorporated into the purely Heisenberg, i.e., exchange only, theories. Bruce and Aharony²² have attempted to explore this question by applying Wilson's renormalization-group theory to a Heisenberg ferromagnet in which dipolar interactions are also included. Close to T_C they find the system "crosses over" to dipolar behavior. According to their calculations, this should occur at a reduced temperature of 0.05 for EuO and 0.10 for EuS. Surprisingly, their results show no evidence of a decrease in the value of γ from 1.375, the Heisenberg value, to a value nearer 1.0, the expected (mean-field) result.

Further calculations by Natterman and Trimper²³ and by Bruce, Kosterlitz, and Nelson²⁴ re-

veal that the situation is actually very complicated. What appears to happen is that within a restricted temperature range near T_C dipolar interactions do in fact reduce the effective value of γ . For EuO, the greatest reduction—about 5%—is estimated to occur at reduced temperatures of 0.001–0.01, not far from the experimentally accessible limits. At reduced temperatures very much smaller or larger than 0.001, dipolar influences are negligible. The low values of γ observed in bulk experiments can thus be understood as resulting from the dipolar crossover. At this time, however, it is still not clear what effect the dipolar crossover will have on the neutron measurements which were made at finite values of q but within roughly the same reduced temperature range as the bulk experiments.

In their calculations, Bruce and Aharony also considered what effect dipolar interactions might have on $\chi_q(T)$ within the experimentally accessible q range, i.e., $0.2 < q/\kappa_1 < 5$. Unfortunately, the authors were not able to make quantitative estimates, remarking only that "deviations from the Ornstein-Zernike form could be quite large." Clearly this is a point which should be further investigated both theoretically and, if possible, experimentally.

Before leaving the subject of comparisons with theory, however, let us briefly turn to the question of what information is available concerning the critical parameters below T_C . The only directly applicable analysis we have been able to find is that of Stephenson and Wood²⁵ who calculated the coefficient B and the exponent β of Eq. (8) using a low-temperature series expansion. Their results are included in Table IV.

Concerning other quantities of interest, scaling arguments predict that both γ and ν will have the same value above and below T_C .²⁶ Also Schofield, Litster, and Ho²⁷ have proposed (on the basis of Schofield's parametric equation of state) that

$$\frac{C^+}{C^-} = \frac{\gamma}{\beta} \left(\frac{(1 - 2\beta)\gamma}{2\beta(\gamma - 1)} \right)^{\gamma-1},$$

where C^+ is the critical coefficient above T_C , defined by Eq. (6), and C^- is its counterpart below T_C . It is easy to show²⁸ that $C^+/C^- = (F^-/F^+)^{2-\eta}$, hence the above expression also relates the critical coefficients F^+ and F^- as defined, respectively, by Eq. (7) and its counterpart below T_C .

Substituting the values for β and γ listed in the next to last column of Table IV in the above expression we obtain 3.95 for the ratio C^+/C^- and 2.02 for the ratio F^-/F^+ . The latter is to be compared with the experimental value of 2.4 obtained from the data of Fig. 7. While the agreement is not particularly good it is probably not outside the

systematic uncertainty of the experimental result, which is large for the reasons discussed in Sec. IV D.

VII. SUMMARY

In general, our investigations of neutron scattering in EuO and EuS confirm the predictions of Heisenberg-model calculations both for short-range order above T_C and for long-range order below T_C . In each case we find that the measured values of the critical coefficients and exponents agree with the predicted values to within the limits of error or nearly so. The expected scaling of the spin correlation range with nearest-neighbor distance is also observed.

As far as short-range order below T_C is concerned, our studies were less conclusive. Here we were faced with the problem of identifying and separating contributions to the scattering from longitudinal and transverse spin fluctuations as well as a background of small-angle scattering, which we believe to be associated with multiple

refraction by magnetic domains. Although our analysis of the data appears to be reasonable, we have not been able to establish that it represents a definitive determination of the parameters involved. Assuming, however, that we have identified the scattering associated with the longitudinal susceptibility correctly, we find the inverse spin correlation range to be about 2.4 times larger below T_C than it is at an equivalent temperature above T_C , a value in reasonable accord with theoretical expectations.

In general, comparisons of the critical parameters derived from our measurements with those obtained by other methods are satisfactory. The only exception worthy of comment is the value of the critical exponent γ , for which the bulk measured value is significantly below our neutron result. Present indications are that at least part of the difficulty can be explained in terms of long-range dipolar interactions, although final judgment on this point should be reserved in view of the fact that dipolar effects are, as yet, imperfectly understood.

*Research sponsored by the U. S. Energy Research and Development Administration.

†Part of the work done while Guest Scientists at Brookhaven National Laboratory.

¹A. Tucciarone, H. Y. Lau, L. M. Corliss, A. Delapalme, and J. M. Hastings, *Phys. Rev. B* **4**, 3206 (1971).

²J. Als-Nielsen, O. W. Dietrich, W. Kummamm, and L. Passell, *Phys. Rev. Lett.* **27**, 741 (1971).

³W. Marshall and S. W. Lovesey, *Theory of Thermal Neutron Scattering* (Oxford U. P., London, 1971).

⁴K. Kawasaki, *Prog. Theor. Phys.* **38**, 1052 (1967).

⁵D. S. Ritchie and M. E. Fisher, *Phys. Rev. B* **5**, 2668 (1972).

⁶J. Als-Nielsen, *Phys. Rev. Lett.* **25**, 730 (1970).

⁷P. Résibois and C. Piette, *Phys. Rev. Lett.* **24**, 514 (1970).

⁸D. T. Teaney, in *Critical Phenomena*, NBS Misc. Publ. No. 273 (U. S. GPO, Washington, D. C., 1966).

⁹G. G. Low, *Proc. Phys. Soc. (Lond.)* **82**, 992 (1963).

¹⁰J. Høg and T. Johansson, *Int. J. Mag.* **4**, 11 (1973).

¹¹N. Menyuk, K. Dwight, and T. B. Reed, *Phys. Rev. B* **3**, 1689 (1971).

¹²G. Groll, *Z. Phys.* **243**, 60 (1971).

¹³C. C. Huang and J. T. Ho, *Phys. Rev. B* **12**, 5255 (1975).

¹⁴P. Heller and G. Benedek, *Phys. Rev. Lett.* **14**, 71 (1965).

¹⁵C. Domb and M. F. Sykes, *Proc. R. Soc. A* **240**, 214 (1957).

¹⁶G. Baker, *Phys. Rev.* **124**, 768 (1967).

¹⁷K. G. Wilson, *Phys. Rev. B* **4**, 3174 (1971); **4**, 3184 (1971).

¹⁸B. Widom, *J. Chem. Phys.* **43**, 3898 (1965).

¹⁹L. P. Kadanoff, *Physics (N.Y.)* **2**, 263 (1966).

²⁰K. G. Wilson and M. E. Fisher, *Phys. Rev. Lett.* **28**, 240 (1972).

²¹A. S. Arrott, B. Heinrich, and J. E. Noakes, *AIP Conf. Proc.* **10**, 822 (1973).

²²A. D. Bruce and A. Aharony, *Phys. Rev. B* **10**, 2078 (1974).

²³T. Nattermann and S. Trimper, *Phys. Lett. A* **50**, 307 (1974).

²⁴A. D. Bruce, J. M. Kosterlitz, and D. R. Nelson, *J. Phys. C* **9**, 825 (1976).

²⁵R. L. Stephenson and P. J. Wood, *J. Phys. C* **3**, 90 (1970).

²⁶H. E. Stanley, *Introduction to Phase Transitions and Critical Phenomena* (Oxford U. P., London, 1971).

²⁷P. Schofield, J. D. Litster, and J. T. Ho, *Phys. Rev. Lett.* **23**, 1098 (1969).

²⁸This follows from Eq. (6.2) of Ref. 5.

²⁹A. Kornblit, G. Ahlers, and E. Buehler, *Phys. Lett. A* **43**, 531 (1973).